The Astrophysical Journal, 634:L57–L60, 2005 November 20

HIGH-MASS STARLESS CORES

T. K. Sridharan,[1] H. Beuther,[1,2] M. Saito,[3] F. Wyrowski,[4] and P. Schilke[4]
Received 2005 June 13; accepted 2005 October 7; published 2005 November 4

ABSTRACT

We report the identification of a sample of potential high-mass starless cores (HMSCs). The cores were discovered by comparing images of fields containing candidate high-mass protostellar objects (HMPOs) at 1.2 mm and mid-infrared (MIR; 8.3 μm) wavelengths. While the HMPOs are detected at both wavelengths, several cores emitting at 1.2 mm in the same fields show absorption or no emission at the MIR wavelength. We argue that the absorption is caused by cold dust. The estimated masses of a few times 10^2–10^3 $M_\odot$ and the lack of IR emission suggest that they may be massive cold cores in a prestellar phase, which could form massive stars. Ammonia observations indicate smaller velocity dispersions and lower rotation temperatures compared with HMPOs and ultracompact H II regions, suggesting a quiescent prestellar stage. We propose that these newly discovered cores are good candidates for the HMSC stage in high-mass star formation. This sample of cores will allow us to study the high-mass star and cluster formation processes at the earliest evolutionary stages.

Subject headings: dust, extinction — infrared: ISM — ISM: clouds — ISM: molecules — ISM: structure — stars: formation

1. INTRODUCTION

The area of high-mass star formation is witnessing significant progress. Systematic studies have uncovered several high-mass protostellar objects (HMPOs) in a pre–ultracompact (UC) H II region phase (Molinari et al. 1996, 2002; Sridharan et al. 2002; Beuther et al. 2002a). The ubiquity of the outflows in these objects points to essential similarities between the high- and the low-mass star formation processes, namely, the presence of a disk accretion phase (Zhang et al. 2005; Beuther et al. 2002b). The characteristics of the high-mass starless core (HMSC) stage, which must precede the HMPO stage, have barely been studied (Evans et al. 2002), in contrast to low-mass starless cores, for which recent studies are constraining the initial conditions for star formation (Motte et al. 1998; Bacmann et al. 2000; Alves et al. 2001; Harvey et al. 2003). Studies of HMSCs are important to answer a central question in star formation: How do star formation processes produce the stellar initial mass function? Since high-mass stars form in clusters, and a major fraction of all stars form in such environments, the structure of the HMSCs represents the initial conditions for general star formation. In this Letter, we present and study a sample of potential HMSCs identified by combining images at millimeter and mid-infrared wavelengths of HMPO fields. The candidate HMSCs belong to the general class of infrared-dark clouds (IRDCs), studied recently by others (Pérault et al. 1996; Egan et al. 1998; Carey et al. 2000; Bacmann et al. 2000; Teyssier et al. 2002; Garay et al. 2004). In the following, we use the terms *starless* and *prestellar* to indicate the lack of massive star formation ($\gtrsim$8 $M_\odot$; spectral type B2 or earlier), and the objects discussed are *candidates* to be in the HMSC stage.

[1] Harvard-Smithsonian Center for Astrophysics, Mail Stop 78, 60 Garden Street, Cambridge, MA 02138; tksridha@cfa.harvard.edu.

[2] Current address: Max-Planck-Institut für Astronomie, Königstuhl 17, D-69117 Heidelberg, Germany; beuther@mpia-hd.mpg.de.

[3] National Astronomical Observatory of Japan, 2-21-1 Osawa, Mitaka, Tokyo 181-8588, Japan; Masao.Saito@nao.ac.jp.

[4] Max-Planck-Institut für Radioastronomie, Auf dem Hügel 69, D-53121 Bonn, Germany; schilke@mpifr-bonn.mpg.de, wyrowski@mpifr-bonn.mpg.de.

2. SOURCE SAMPLE

Continuum images at 1.2 mm and 8.3 μm wavelengths of a sample of 69 HMPOs that we have been studying (Sridharan et al. 2002; Beuther et al. 2002a, 2002b; Williams et al. 2004, 2005) were used to identify the HMSCs. The 1.2 mm images, obtained with the IRAM 30 m telescope, have been described in detail in Beuther et al. (2002a). The 8.3 μm images are archival data from the *Midcourse Space Experiment* (*MSX*; Egan et al. 1998).[5]

The 1.2 mm images, each covering a $\sim 5' \times 5'$ field around an HMPO, detected multiple sources in a number of fields, with an average multiplicity rate of 2.2 (Beuther et al. 2002a). We argued in Sridharan et al. (2002) and Beuther et al. (2002a) that the objects in our HMPO sample are likely to be in various stages of evolution because of the clustered mode of high-mass star formation. Motivated by the possibility of an earlier starless stage in the high-mass star formation process occurring in the same fields, we compared the 1.2 mm and the *MSX* band A (8.3 μm) images of the HMPO fields. Strong emission at the two wavelengths was found to be typical of the HMPOs, with significant position offsets being explained in terms of a cluster setting and varying evolutionary stages (Sridharan et al. 2002). However, in many fields, we also discovered 1.2 mm emission features associated with either *MSX* absorption or no detectable emission, as shown in Figure 1. The strongest millimeter emission near the center of the field in Figure 1*a*, also detected at 8.3 μm, is associated with the HMPO IRAS 18385−0512. The millimeter emission feature to the southeast of the HMPO is associated with absorption at 8.3 μm. Figure 1*b* (the HMPO IRAS 18223−1243; also studied by Garay et al. 2004) and Figure 1*c* indicate the range of morphologies, showing filamentary structures and a field of multiple cores where a stellar cluster may be forming. Following similar observations of low-mass starless cores (e.g., Bacmann et al. 2000), we suggest that the absorption is caused by the same cold dust emitting at 1.2 mm. The similarity of the morphologies of the emission and absorption supports this. In the case of the IRDC 18385−0512-3 (Fig. 1*a*), using a temperature of 15 K

[5] Available at the *MSX* Web site (http://www.ipac.caltech.edu/ipac/msx/msx.html).

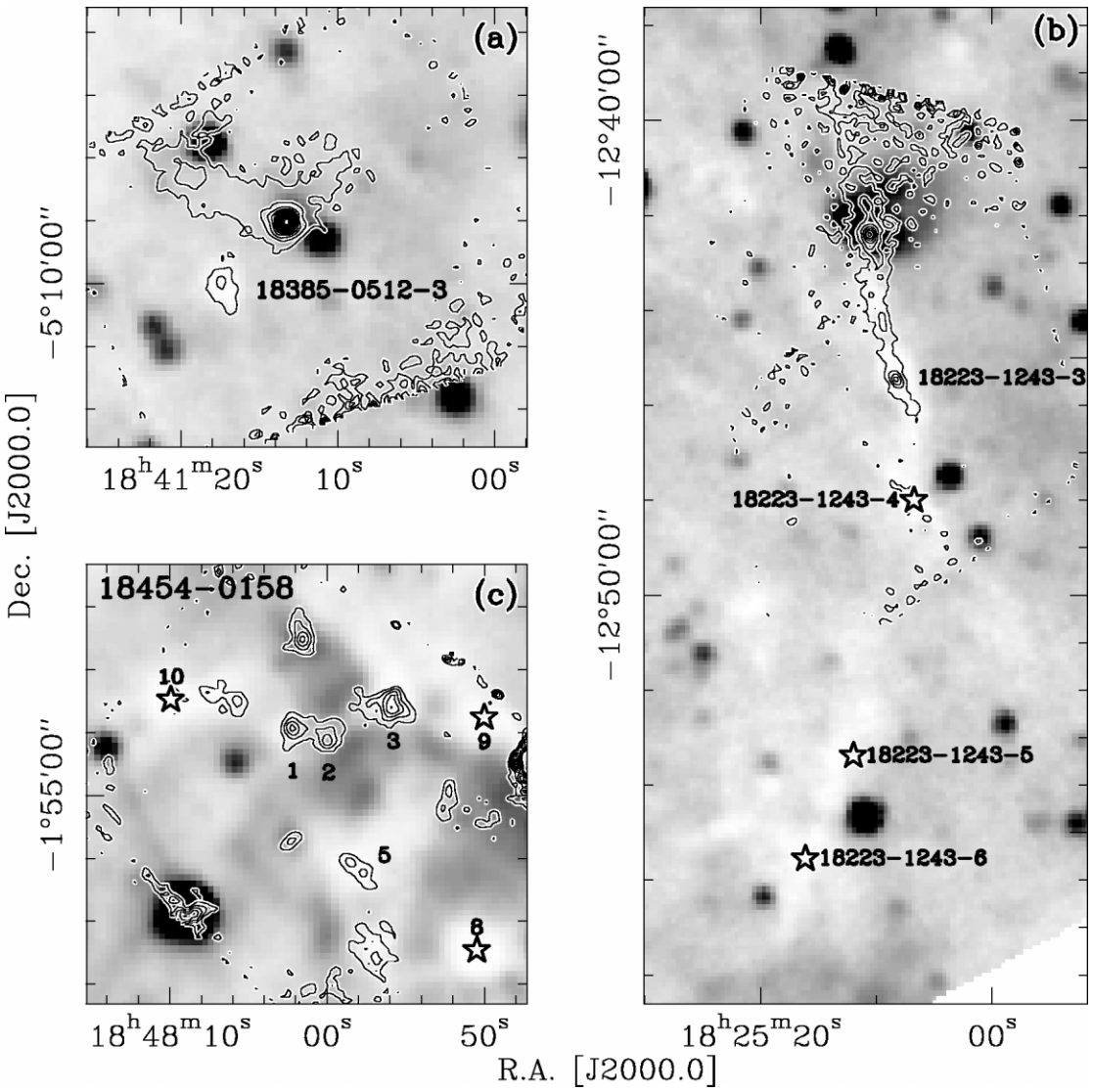

FIG. 1.—*MSX* A-band (8 μm) images (black is bright) with 1.2 mm emission contours: (*a*) IRDC 18385−0512-3; (*b*, *c*) fields 18223−1243 and 18454−0158, with filaments and multiple cores. The five-pointed stars mark cores lacking good 1.2 mm measurements.

(see § 3) and the 1.2 mm flux, a mass of 344 $M_\odot$ is estimated, making it a potential high-mass starless core.

We have identified a total of 56 candidate HMSCs, listed in Table 1 along with kinematic distances, 1.2 mm fluxes, and masses. Each object is labeled with the HMPO field and the millimeter-emission clump number from Beuther et al. (2002a). We have included 26 prominent *MSX* absorption objects lying either outside the 1.2 mm images or where the images are too noisy, extending the numbering. For mass estimates (30 objects), as for the HMPOs (Beuther et al. 2002a, 2005; Hildebrand 1983), we used a value of 2 for the spectral index of dust emissivity β, 100 for the gas-to-dust ratio, 0.1 μm for grain size, and 3 g cm^{-3} for grain mass density ($\kappa = 0.4$ cm^2 per gram of dust), and a temperature of 15 K (§ 3). In case of distance ambiguity, the near distance has been used—at the far distance, MIR absorption is unlikely. The cores are massive, with masses in the range of a few times 10^2–10^3 $M_\odot$.

An examination of the *IRAS* high-resolution processed (HIRES) images (Aumann et al. 1990) of the fields failed to detect any emission from dust heated by star formation activity. Based on the Arcetri Catalog of water masers (Valdettaro et al. 2001), the General Catalogue of 6.7-GHz Methanol Masers (Pestalozzi et al. 2005), and interferometric maser observations of the HMPO fields (Beuther et al. 2002c), we find two cases, IRAS 18102−1800-1 and IRAS 18151−1208-2, to be associated with methanol and water maser emission, respectively, implying star formation in these cores. This suggests that the sample presented here contains cores in multiple evolutionary stages. However, all these stages represent phases before the pre–UC H II/HMPO phase, containing either low-mass young stellar objects or early precursors to the HMPOs. A further implication is that the maser activity may turn on very early in the star formation process, and a majority of the cores presented here may be in an even younger phase.

3. OBSERVATIONS, RESULTS, AND DISCUSSION

To characterize the state of the dense gas in the sample, 34 objects from Table 1 were observed with the Effelsberg 100 m telescope for NH_3 emission in 2002 December. The (1, 1) and (2, 2) lines were detected toward all the sources, observing in frequency-switched mode with a velocity resolution of 0.25 km s^{-1} and ~4 minutes of integration time per position. For 18 sources with good-quality spectra, rotation temperatures

TABLE 1
CANDIDATE HIGH-MASS STARLESS CORES

No.	IRDC	R.A. (J2000.0)	Decl. (J2000.0)	D (kpc)	$S_{1.3}$ (Jy)	v_{lsr} (km s^{-1})	Δv (km s^{-1})	T (K)	$M_{15\,K}$ ($M_\odot$)
1	IRAS 18089−1732-3	18 11 45.3	−17 30 38	3.6	0.3	34.1	2.2	15.6	241
2	IRAS 18090−1832-2	18 12 02.0	−18 31 27	6.6	0.2	…	…	…	541
3	IRAS 18102−1800-1	18 13 11.0	−18 00 23	2.6	3.3	14.0	…	…	1385
4	IRAS 18151−1208-2	18 17 50.3	−12 07 54	3.0	2.6	29.3	2.2	18.5	1453
5	IRAS 18182−1433-2	18 21 14.9	−14 33 06	3.6[a]	0.3	40.5	1.4	15.5	241
6	IRAS 18182−1433-3	18 21 17.5	−14 29 43	…	…	59.4	1.2	…	…
7	IRAS 18182−1433-4	18 21 14.0	−14 34 20	…	…	…	…	…	…
8	IRAS 18223−1243-2	18 25 10.0	−12 44 00	3.7	0.6	…	…	…	510
9	IRAS 18223−1243-3	18 25 08.3	−12 45 27	3.7	0.8	45.3	2.2	32.7	245[b]
10	IRAS 18223−1243-4	18 25 06.8	−12 48 00	3.7	0.3	45.4	1.4	13.0	255
11	IRAS 18223−1243-5	18 25 12.0	−12 53 23	…	…	44.7	1.1	…	…
12	IRAS 18223−1243-6	18 25 16.2	−12 55 33	…	…	45.3/50.5	1.4/2.1	…	…
13	IRAS 18247−1147-3	18 27 31.0	−11 44 46	6.7	0.4	…	…	…	1115
14	IRAS 18264−1152-2	18 29 21.0	−11 51 55	…	…	…	…	…	…
15	IRAS 18264−1152-3	18 29 27.0	−11 50 58	…	…	…	…	…	…
16	IRAS 18306−0835-3	18 33 32.1	−08 32 28	2.5[a]	0.8	31.6	1.6	13.1	310
17	IRAS 18306−0835-4	18 33 34.8	−08 31 20	…	…	32.1	2.0	…	…
18	IRAS 18308−0841-2	18 33 34.3	−08 38 42	4.9	0.6	…	…	…	895
19	IRAS 18308−0841-3	18 33 29.3	−08 38 17	4.9	0.7	73.7	1.9	16.2	1044
20	IRAS 18308−0841-5	18 33 34.4	−08 37 36	4.9	0.2	76.7	1.5	14.5	298
21	IRAS 18308−0841-6	18 33 34.9	−08 36 04	…	…	76.9	1.6	…	…
22	IRAS 18310−0825-4	18 33 39.5	−08 21 10	5.2	0.5	86.5	1.7	18.3	840
23	IRAS 18337−0743-3	18 36 18.2	−07 41 00	4.0	0.3	55.6	1.8	15.6	298
24	IRAS 18337−0743-4	18 36 29.9	−07 42 05	…	…	55.2	2.1	…	…
25	IRAS 18337−0743-5	18 36 41.0	−07 39 56	…	…	…	…	…	…
26	IRAS 18337−0743-6	18 36 36.0	−07 42 17	…	…	…	…	…	…
27	IRAS 18337−0743-7	18 36 19.0	−07 41 48	…	…	…	…	…	…
28	IRAS 18348−0616-8	18 37 14.7	−06 17 25	…	…	109.2	…	…	…
29	IRAS 18348−0616-2[c]	18 37 27.6	−06 14 08	6.3	0.5	…	…	…	1232
30	IRAS 18385−0512-3	18 41 17.4	−05 10 03	4.3[a]	0.3	66.7	1.1	14.4	344
31	IRAS 18431−0312-3	18 45 45.0	−03 08 56	…	…	…	…	…	…
32	IRAS 18431−0312-4	18 45 53.0	−03 09 01	…	…	…	…	…	…
33	IRAS 18437−0216-3	18 46 21.9	−02 12 24	6.6[d]	0.3	110.2/96.4	1.4/1.24	15.9/13.8	811
34	IRAS 18437−0216-7	18 46 22.0	−02 14 10	…	…	…	…	…	…
35	IRAS 18440−0148-2	18 46 31.0	−01 47 08	…	…	…	…	…	…
36	IRAS 18445−0222-4	18 47 14.6	−02 15 44	…	…	88.2	1.0	…	…
37	IRAS 18447−0229-3	18 47 42.0	−02 25 12	…	…	101.0	1.1	…	…
38	IRAS 18447−0229-4	18 47 38.9	−02 28 00	…	…	98.6/111.8	1.3	…	…
39	IRAS 18447−0229-5	18 47 31.4	−02 26 46	…	…	104.0	1.2	…	…
40	IRAS 18454−0158-1	18 48 02.1	−01 53 56	4.7[d]	0.4	51.9/99.6	1.5/1.9	…	549
41	IRAS 18454−0158-3	18 47 55.8	−01 53 34	6.0[a]	0.7	93.7/97.6	…	…	1565
42	IRAS 18454−0158-5	18 47 58.1	−01 56 10	6.0[a]	0.3	93.9	1.5	17.6	671
43	IRAS 18454−0158-8	18 47 50.5	−01 57 28	…	…	94.6	…	…	…
44	IRAS 18454−0158-9	18 47 50.0	−01 53 46	…	…	95.6/101.8	…	…	…
45	IRAS 18454−0158-10	18 48 10.0	−01 53 29	…	…	100.4	…	…	…
46	IRAS 18454−0158-11	18 48 07.0	−01 53 25	…	…	…	…	…	…
47	IRAS 18454−0158-12	18 48 05.7	−01 53 28	…	…	…	…	…	…
48	IRAS 18460−0307-3	18 48 36.0	−03 03 49	5.2	0.3	…	…	…	504
49	IRAS 18460−0307-4	18 48 46.0	−03 04 05	5.2	0.3	…	…	…	504
50	IRAS 18460−0307-5	18 48 47.0	−03 01 29	5.2	0.5	…	…	…	840
51	IRAS 18530+0215-2	18 55 29.0	+02 17 43	…	…	…	…	…	…
52	IRAS 19175+1357-3[e]	19 19 52.1	+14 01 52	1.1[a]	0.2	7.7	1.5	15.6	15
53	IRAS 19175+1357-4[e]	19 19 50.6	+14 01 22	1.1[a]	0.2	7.7	1.5	13.2	15
54	IRAS 19410+2336-2	19 43 10.2	+23 45 04	2.1	1.4	21.4	2.0	18.3	383
55	IRAS 20081+2720-1[e]	20 10 13.0	+27 28 18	0.7	0.6	5.5	…	…	18
56	IRAS 22570+5912-3	22 58 55.1	+59 28 33	5.1	0.5	−47.1	2.6	16.2	807

NOTE.—Units of right ascension are hours, minutes, and seconds, and units of declination are degrees, arcminutes, and arcseconds.
[a] Different velocities, kinematic distances, and masses compared with those in Sridharan et al. (2002) and Beuther et al. (2002b).
[b] A dust temperature of 32.7 K was used to compute this mass, a significantly higher temperature than the rest of the sample.
[c] The right ascension reported in Beuther et al. (2002b) for this object is in error by ∼30″.
[d] An average of the kinematic distances for the two velocity components.
[e] May not qualify as high-mass; included for completeness.

were derived (Ungerechts et al. 1986). Figure 2 shows an example NH_3 (1, 1) spectrum, for IRAS 18385−0512-3, whose image is shown in Figure 1*a*. This core has a small line width of 1.1 km s^{-1}.

Figure 3 compares the ammonia line widths and rotation temperatures for the HMSCs, HMPOs, and UC H II regions (Sridharan et al. 2002; Churchwell et al. 1990). The HMSCs show a smaller median line width of 1.5 km s^{-1} (mean 1.6 km s^{-1}) compared with 1.9 km s^{-1} (mean 2.1 km s^{-1}) for the HMPOs. This suggests smaller internal motions and therefore more quiescent conditions, supporting the prestellar nature of the HMSCs. The median rotation temperature of 16.9 K (mean 15.3 K) indicates colder conditions in the HMSCs compared with 18.5 K (mean 22.5 K) for HMPOs, again suggesting

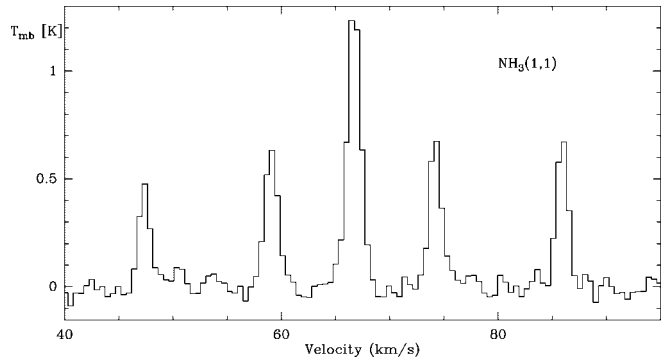

FIG. 2.—An NH_3 (1, 1) spectrum for IRAS 18385−0512-3.

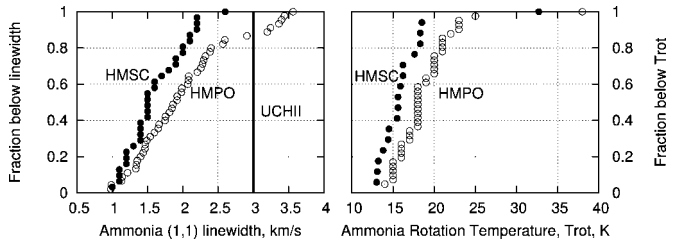

FIG. 3.—*Left*, cumulative distributions of NH_3 (1, 1) line widths for HMSCs and HMPOs, with the median for UC H II regions shown as a vertical line; *right*, cumulative distributions of NH_3 rotation temperatures for HMSCs and HMPOs.

a quiescent stage. The corresponding ammonia line widths and temperatures for UC H II regions are 3 km s^{-1} and 22 K (Churchwell et al. 1990). These results support the picture in which the objects evolve from HMSCs to HMPOs to UC H II regions.

Although the ammonia rotation temperatures for the HMSCs are only marginally lower than for the HMPOs, where graybody dust temperatures were estimated to be much higher (Sridharan et al. 2002), we believe that the dust in the HMSCs is cooler and well characterized by the gas temperature. For the HMPOs, the best fits to the spatial and the spectral energy distributions at far-infrared (FIR) and millimeter wavelengths imply temperatures increasing inward (Williams et al. 2005). Ammonia emission traces the cooler outer regions, leading to lower rotation temperature estimates. In contrast, for externally heated HMSCs the dust and gas temperatures are expected to be similar in the outer regions. (Li et al. 2003). The lack of FIR emission toward the HMSCs—in cases where the dominant HMPO in the field is not nearby, no emission is seen even at 60 μm or 100 μm wavelengths in the HIRES images—indicates the absence of dust heated by an embedded object.

The distributions of ammonia rotation temperatures and line widths of the HMSCs and the HMPOs were subjected to a Kolmogorov-Smirnov test, resulting in 0.90 and 0.62 for the probabilities that they are different. The masses of HMSCs are distributed over a similar range as the HMPOs. Virial masses estimated from ammonia line widths and 1.2 mm sizes are lower than but comparable to dust-derived masses, consistent with the HMSCs' being in equilibrium. Because of the many uncertainties in mass estimates in both the cases, we do not make further comparisons.

An upper limit to the luminosity of an embedded star of $\sim$100 $L_\odot$ is derived from the *IRAS* flux limits, for a distance of 4 kpc, corresponding to early A spectral types ($\sim$2–3 $M_\odot$). Assuming a star formation efficiency of 30%, an HMSC mass of 550 $M_\odot$ (sample median), and an initial mass function with power-law indices 2.3 and 1.3 for masses greater than 0.5 and 0.08–0.5 $M_\odot$, respectively (Kroupa 2004), we estimate that one star of mass $\gtrsim$20 $M_\odot$ could form in an HMSC. While there is no current evidence for massive star formation in these cores from their infrared fluxes, more sensitive searches such as the *Spitzer* GLIMPSE survey will presumably uncover lower mass star formation or hitherto unknown early stages of high-mass star formation.

In summary, we have identified a sample of candidate high-mass starless cores, likely to contain objects in multiple stages of evolution prior to the formation of massive stars. The sample provides an opportunity to determine initial conditions for high-mass star/cluster formation and star formation in general. Multiwavelength studies of their internal structure with instruments such as the Submillimeter Array and the *Spitzer Space Telescope* will help in understanding the origin of the stellar initial mass function, a central puzzle in star formation.

H. B. thanks the Emmy Noether Programme, Deutsche Forschungsgemeinschaft, for support (grant BE2578/1).

REFERENCES

Alves, J. F., Lada, C. J., & Lada, E. A. 2001, Nature, 409, 159
Aumann, H. H., Fowler, J. W., & Melnyk, M. 1990, AJ, 99, 1674
Bacmann, A., André, P., Puget, J.-L., Abergel, A., Bontemps, S., & Ward-Thompson, D. 2000, A&A, 361, 555
Beuther, H., Schilke, P., Menten, K. M., Motte, F., Sridharan, T. K., & Wyrowski, F. 2002a, ApJ, 566, 945
———. 2005, ApJ, 633, 535
Beuther, H., Schilke, P., Sridharan, T. K., Menten, K. M., Walmsley, C. M., & Wyrowski, F. 2002b, A&A, 383, 892
Beuther, H., Walsh, A., Schilke, P., Sridharan, T. K., Menten, K. M., & Wyrowski, F. 2002c, A&A, 390, 289
Carey, S. J., Feldman, P. A., Redman, R. O., Egan, M. P., MacLeod, J. M., & Price, S. D. 2000, ApJ, 543, L157
Churchwell, E., Walmsley, C. M., & Cesaroni, R. 1990, A&AS, 83, 119
Egan, M. P., Shipman, R. F., Price, S. D., Carey, S. J., Clark, F. O., & Cohen, M. 1998, ApJ, 494, L199
Evans, N. J., II, Shirley, Y. L., Mueller, K. E., & Knez, C. 2002, in ASP Conf. Ser. 267, Hot Star Workshop III, ed. P. A. Crowther (San Francisco: ASP), 17
Garay, G., Faúndez, S., Mardones, D., Bronfman, L., Chini, R., & Nyman, L.-Å. 2004, ApJ, 610, 313
Harvey, D. W. A., Wilner, D. J., Lada, C. J., Myers, P. C., & Alves, J. F. 2003, ApJ, 598, 1112
Hildebrand, R. H. 1983, QJRAS, 24, 267
Kroupa, P. 2004, NewA Rev., 48, 47
Li, D., Goldsmith, P. F., & Menten, K. 2003, ApJ, 587, 262
Molinari, S., Brand, J., Cesaroni, R., & Palla, F. 1996, A&A, 308, 573
Molinari, S., Testi, L., Rodríguez, L. F., & Zhang, Q. 2002, ApJ, 570, 758
Motte, F., André, P., & Neri, R. 1998, A&A, 336, 150
Pérault, M., et al. 1996, A&A, 315, L165
Pestalozzi, M. R., Minier, V., & Booth, R. S. 2005, A&A, 432, 737
Sridharan, T. K., Beuther, H., Schilke, P., Menten, K. M., & Wyrowski, F. 2002, ApJ, 566, 931
Teyssier, D., Hennebelle, P., & Pérault, M. 2002, A&A, 382, 624
Ungerechts, H., Walmsley, C. M., & Winnewisser, G. 1986, A&A, 157, 207
Valdettaro, R., et al. 2001, A&A, 368, 845
Williams, S. J., Fuller, G. A., & Sridharan, T. K. 2004, A&A, 417, 115
———. 2005, A&A, 434, 257
Zhang, Q., Hunter, T. R., Brand, J., Sridharan, T. K., Cesaroni, R., Molinari, S., Wang, J., & Kramer, M. 2005, ApJ, 625, 864